Highlights

- Neural trajectories in the hippocampus exhibited greater variability during a working memory (WM) task compared to those in the entorhinal cortex and amygdala regions.

- The distance of neural trajectories between encoding and retrieval states in the hippocampus was memory-load dependent during a WM task.

- Hippocampal neural trajectories fluctuated between the encoding and retrieval states in a task-dependent manner during both baseline and sharp-wave ripple (SWR) periods.

- Hippocampal neural trajectories shifted from encoding to retrieval states during SWR period.

Hippocampal neural fluctuations between memory encoding and retrieval states during a working memory task in humans

Yusuke Watanabe[a,*], Yuji Ikegaya[b,c,d], Takufumi Yanagisawa[a,e]

[a]*Institute for Advanced Cocreation studies, Osaka University, 2-2 Yamadaoka, Suita, 565-0871, Osaka, Japan*
[b]*Graduate School of Pharmaceutical Sciences, The University of Tokyo, 7-3-1 Hongo, Tokyo, 113-0033, Japan*
[c]*Institute for AI and Beyond, The University of Tokyo, 7-3-1 Hongo, Tokyo, 113-0033, Japan*
[d]*Center for Information and Neural Networks, National Institute of Information and Communications Technology, 1-4 Yamadaoka, Suita City, 565-0871, Osaka, Japan*
[e]*Department of Neurosurgery, Osaka University Graduate School of Medicine, 2-2 Yamadaoka, Osaka, 565-0871, Japan*

Abstract

Working memory (WM) plays a critical role in ~~many~~ various cognitive functions, but the intricate neural mechanisms that support its operation remain elusive. Specifically, while the hippocampus and sharp-wave ripple complexes (SWRs) – brief, synchronous neural oscillation observed in the hippocampus – are recognized for their roles in memory consolidation and retrieval, their involvement in WM tasks has not yet been defined. ~~Current research suggests that during WM tasks~~Here we show that during a WM task, multiunit activity patterns in the hippocampus display distinctive dynamics, particularly during SWR periods. This study analyzed a dataset derived from intracranial electroencephalogram recordings ~~made~~ conducted in the medial temporal lobe (MTL) of nine individuals with epilepsy during an eight-second Sternberg task. We applied Gaussian-process factor analysis to determine low-dimensional neural representations, or 'trajectories,' within the MTL regions while performing the WM task. The results ~~indicate~~ revealed significant variations in the hippocampus' neural trajectories compared to those in the entorhinal cortex and amygdala. Additionally, the distance of the trajectory between the encoding and retrieval phases was dependent on memory load. Importantly, hippocampal trajectories during the retrieval phase demonstrated ~~variations~~ fluctuations between encoding and retrieval stages based on task type, particularly showing ~~shifts~~transient shift from encoding to retrieval states during SWRs. These findings underline the hippocampus's essential function in performing WM tasks and propose ~~an intriguing~~ a hypothesis for future research: the functional state of the hippocampus transition from encoding to retrieval during SWRs.

Keywords: working memory, memory load, hippocampus, sharp-wave ripples, humans

1. Introduction

Working memory (WM) significantly influences everyday life, and the neural bases of this cognitive process continue to be the subject of intensive research. One key focus of this research is the hippocampus, a structure integral to memory functions [1] [2] [3] [4] [5] [6] [7] [8] [9]. A ~~thorough~~ deeper understanding of the hippocampus's role in working memory is ~~essential~~ not only crucial for advancing our knowledge ~~of cognitive processes CHECKME>~~and fostering advancements in cognitive training and interventions<CHECKME ENDSbut also potentially for enhancing cognitive abilities.

Current evidence suggests that a transient, synchronized oscillation, called sharp-wave ripple (SWR) [10], is associated with several cognitive functions. These include memory replay [11] [12] [13] [14] [15], memory consolidation [16] [17] [18] [19], memory recall [20] [21] [22], and neural plasticity [23] [24]. ~~This association suggests~~ These associations suggest that SWR may be a ~~crucial part~~ fundamental computational manifestation of hippocampal processing~~that contributes~~, contributing to working memory

*Corresponding author. Tel: +81-6-6879-3652

performance as well. However, research on the effects of SWRs on working memory is relatively scarce [25], and is predominantly limited to rodent models engaged in navigation tasks, where the timing of memory acquisition and recall is not clearly defined.

Recent studies have found low-dimensional representations in the hippocampal neurons can explain WM task performances. Specifically, the firing patterns of place cells [26] [27] [28] [29] [30], found in the hippocampus, have been identified within a dynamic, nonlinear three-dimensional hyperbolic space in rats [31]. Additionally, grid cells in the entorhinal cortex (EC), which is the main pathway to the hippocampus [32] [33] [34], exhibited a toroidal geometry during exploration in rats [35]. However, these studies are limited by their focus on spatial navigation tasks in rodents, affecting the temporal resolution of WM tasks. To illustrate, the timing of when an animal acquires information is ambiguous in these settings. Therefore, the applicability of these findings to human subjects and tasks beyond navigation still requires confirmation.

Considering these factors, this study investigates the hypothesis that hippocampal neurons show unique 'neural trajectories' in low-dimensional spaces, particularly during SWR periods, in response to WM tasks. To test this hypothesis, we employed a dataset of patients performing an eight-second Sternberg task (1 s for fixation, 2 s for encoding, 3 s for maintenance, and 2 s for retrieval) with high temporal resolution. Intracranial electroencephalography (iEEG) signals within the medial temporal lobe (MTL) were recorded for these patients [36]. To examine low-dimensional neural trajectories, we utilized Gaussian-process factor analysis (GPFA), an established method for analyzing neural population dynamics [37].

2. Methods

2.1. Dataset

The dataset used in this study, which is publicly available, comprises nine epilepsy patients performing a modified Sternberg task [36]. This task includes four phases: fixation (1s), encoding (2s), maintenance (3s), and retrieval (2s). During the encoding phase, participants were presented with a set of four, six, or eight alphabet letters. They were then tasked with determining whether a probe letter displayed during the retrieval phase had previously appeared (the correct response for Match IN task) or not (the correct response for Mismatch OUT task). Intracranial electroencephalography (iEEG) signals were captured with a 32 kHz sampling rate within a 0.5–5,000 Hz frequency range, using depth electrodes in medial temporal lobe (MTL) regions: the anterior head of the left and right hippocampus (AHL and AHR), the posterior body of the hippocampus (PHL and PHR), the entorhinal cortex (ECL and ECR), and the amygdala (AL and AR), as depicted in Figure 1A and Table 1. The iEEG signals were subsequently downsampled to 2 kHz. Correlations between variables such as set size and correct rate were examined (Figure S1). Multiunit spike timings were determined via a spike sorting algorithm [38] using the Combinato package (`https://github.com/jniediek/combinato`)(Figure 1C).

2.2. Calculation of neural trajectories using GPFA

Neural trajectories, also referred to as 'factors', in the hippocampus, EC, and amygdala were determined using GPFA [37] applied to the multiunit activity data for each session, performed with the elephant package (`https://elephant.readthedocs.io/en/latest/reference/gpfa.html`). The bin size was set to 50 ms, without overlaps. Each factor was z-normalized across all sessions, and the Euclidean distance from the origin (O) was then computed.

For each trajectory within a region such as AHL, geometric medians (g_F for fixation, g_E for encoding, g_M for maintenance, and g_R for retrieval phase) were calculated by determining the median coordinates of the trajectory during the four phases. An optimal GPFA dimensionality was found to be three using the elbow method obtained by examining the log-likelihood val-

ues through a three-fold cross-validation approach (Figure 2B).

2.3. Identifying SWR candidates from hippocampal regions

Potential SWR events within the hippocampus were detected using a widely used method [39]. LFP signals from a region of interest (ROI) like AHL, were re-referenced by deducting the averaged signal from locations outside the ROI (for instance, AHR, PHL, PHR, ECL, ECR, AL, and AR)(see Figure 1A). The re-referenced LFP signals were then filtered with a ripple-band filter (80–140 Hz) to determine SWR candidates, marked as SWR$^+$ candidates(see Figure 1B). SWR detection was carried out using a published tool (`https://github.com/Eden-Kramer-Lab/ripple_detection`) [40], with the bandpass range adjusted to 80–140 Hz for humans [21] [22], unlike the initial 150–250 Hz range typically applied to rodents.

Control events for SWR$^+$ candidates, labeled as SWR$^-$ candidates, were detected by randomly shuffling the timestamps of SWR$^+$ candidates across all trials and subjects. The resulting SWR$^+$/SWR$^-$ candidates were then visually inspected(Figure 1).

2.4. Defining SWRs from putative hippocampal CA1 regions

Potential SWRs were differentiated from SWR candidates in putative CA1 (cornu Ammonis 1) regions. These regions were initially defined as follows: SWR$^+$/SWR$^-$ candidates in the hippocampus were projected into a two-dimensional space based on overlapping spike counts per unit using a supervised method, UMAP (Uniform Manifold Approximation and Projection) [41](Figure 4A). Clustering validation was performed by calculating the silhouette score [42] from clustered samples(Table 2). Regions in the hippocampus, which scored above 0.6 on average across sessions (75th percentile)(Figure 4B), were identified as putative CA1 regions, resulting in the identification of five electrode positions from five patients(Table 3).

SWR$^+$/SWR$^-$ candidates in these predetermined CA1 regions were categorized as SWR$^+$/SWR$^-$, and thus they no longer retained their candidate status. The duration and ripple band peak amplitude of SWRs were found to follow log-normal distributions(Figure 4C & E). Each time period of SWR was partitioned relative to the time from the SWR center into pre- (at −800 to −300 ms from the SWR center), mid- (at −250 to +250 ms), and post-SWR (at +300 to +800 ms) times.

2.5. Statistical evaluation

Both the Brunner–Munzel test and the Kruskal-Wallis test were executed using the SciPy package in Python [43]. Correlational analysis was conducted by determining the rank of the observed correlation coefficient within its associated set-size-shuffled surrogate using a customized Python script. The bootstrap test was implemented with an in-house Python script.

3. Results

3.1. iEEG recording and neural trajectory in MTL regions during a Sternberg task

Our analysis employed a publicly accessible dataset [36], which comprises LFP signals (Figure 1A) from MTL regions (Table 1) recorded during the execution of a modified Sternberg task. We extracted SWR$^+$ candidates from LFP signals that were filtered in the 80–140 Hz ripple band (Figure 1B), originating in all hippocampal regions (refer to Methods section). Meanwhile, SWR$^-$ candidates, control events for SWR$^+$ candidates, were defined at the same timestamps but distributed across different trials (Figure 1). The dataset also encompassed multiunit spikes (Figure 1C), recognized via a spike sorting algorithm [38]. Employing GPFA [37], we applied this to 50-ms windows of binned multiunit activity without overlaps to determine the neural trajectories, or factors, of MTL regions by session and region (Figure 1D). We normalized each factor per session and region, for instance, session #2 in AHL of subject #1. We then calculated the Euclidean distance from the origin (O) (Figure 1E).

3.2. Hippocampal neural trajectory correlation with a Sternberg task

Figure 2A exhibits a distribution of median neural trajectories, comprising 50 trials, within the three main factor spaces. Utilizing the elbow method, we established the optimal embedding dimension for the GPFA model as three (Figure 2B). The trajectory distance from

the origin (O) ~~—~~ represented as $\|g_F\|$, $\|g_E\|$, $\|g_M\|$, and $\|g_R\|$ ~~—~~ in the hippocampus surpassed the corresponding distances in the EC and amygdala (Figure 2C & D).[1]

Similarly, we computed the distances between the geometric medians of four phases, namely $\|g_Fg_E\|$, $\|g_Fg_M\|$, $\|g_Fg_R\|$, $\|g_Eg_M\|$, $\|g_Eg_R\|$, and $\|g_Mg_R\|$. ~~Our findings suggest that the~~ The hippocampus showed larger distances between phases than those in the EC and amygdala. [2]

3.3. Memory-load-dependent neural trajectory distance between encoding and retrieval states in the hippocampus

Regarding memory load in the Sternberg task, we observed a negative correlation between the correct rate of trials and the set size, which denotes the number of letters to be encoded (Figure 3A).[3] Concomitantly, a positive correlation was noted between the response time and set size (Figure 3B).[4].

Next, we discovered a positive correlation between set size and the trajectory distance separating the encoding and retrieval phases ($\log_{10}\|g_Eg_R\|$) (Figure 3C).[5]. However, distances between other phase combinations did not highlight statistically significant correlations (Figures 3D and **??**).

3.4. Detection of hippocampal SWR from putative CA1 regions

To enhance the precision of recording sites and SWR detection, we approximated the electrode placements in the CA1 regions of the hippocampus using distinguished multiunit spike patterns during SWR events. SWR^+/SWR^- candidates from each session and hippocampal region were embedded in two-dimensional space using UMAP (Figure 4A).[6] With the silhouette score as a quality metric for clustering (Figure 4B and Table 2), recording sites demonstrating an average silhouette score exceeding 0.6 across all sessions were identified as putative CA1 regions.[7] (Tables 2 and 3). We identified five putative CA1 regions, four of which were not indicated as seizure onset zones (Table 1).

Subsequently, SWR^+/SWR^- candidates within these putative CA1 regions were labeled as SWR^+ and SWR^-, respectively[8] (Table 3). Both SWR^+ and SWR^- manifested ~~similar~~ identical durations [9] ~~(Figure 4C)~~ due to their definitions and followed a log-normal distribution (Figure 4C). During the initial 400 ms of the retrieval phase, ~~we noted~~ an increase in SWR^+ incidence was found[10] (Figure 4D). The peak ripple band amplitude of SWR^+ surpassed that of SWR^- and followed a log-normal distribution (Figure 4E).[11]

3.5. Transient changes in hippocampal neural trajectory during SWR

We assessed the 'distance' of the neural trajectory from the origin (O) during SWR events in both encoding and retrieval phases (Figure 5A). Observing the increase in distance during SWR, as illustrated in Figure 5A, we categorized each SWR into three stages: pre-, mid-, and post-SWR. Hence, the distances from O during those SWR intervals are identified as $\|pre\text{-}eSWR^+\|$, $\|mid\text{-}eSWR^+\|$ and others.

---

[1] Hippocampus: Distance = 1.11 [1.01], median [IQR], n = 195,681 timepoints; EC: Distance = 0.94 [1.10], median [IQR], n = 133,761 timepoints; Amygdala: Distance = 0.78 [0.88], median [IQR], n = 165,281 timepoints.

[2] Hippocampus: Distance = 0.60 [0.70], median [IQR], n = 8,772 combinations; EC: Distance = 0.28 [0.52], median [IQR], n = 5,017 combinations ($p < 0.01$; Brunner–Munzel test); Amygdala: Distance = 0.24 [0.42], median [IQR], n = 7,466 combinations ($p < 0.01$; Brunner–Munzel test).

[3] Correct rate: set size four (0.99 ±0.11, mean ±SD; n = 333 trials) vs. set size six (0.93 ±0.26; n = 278 trials; $p < 0.001$, Brunner–Munzel test with Bonferroni correction) and set size eight (0.87 ±0.34; n = 275 trials; $p < 0.05$; Brunner–Munzel test with Bonferroni correction). Generally, $p < 0.001$ for Kruskal–Wallis test; correlation coefficient = - 0.20, $p < 0.001$.

[4] Response time: set size four (1.26 ±0.45 s; n = 333 trials) vs. set size six (1.53 ±0.91 s; n = 278 trials) and set size eight (1.66 ±0.80 s; n = 275 trials). All comparisons $p < 0.001$, Brunner–Munzel test with Bonferroni correction; $p < 0.001$ for Kruskal–Wallis test; correlation coefficient = 0.22, $p < 0.001$

[5] Correlation between set size and $\log_{10}(\|g_Eg_R\|)$: correlation coefficient = 0.05, $p < 0.001$. Specific values: $\|g_Eg_R\|$ = 0.54 [0.70] for set size four, n = 447; $\|g_Eg_R\|$ = 0.58 [0.66] for set size six, n = 381; $\|g_Eg_R\|$ = 0.61 [0.63] for set size eight, n = 395.

[6] Consider the AHL in session #1 of subject #1 as a case in point.

[7] The identified regions were the AHL of subject #1, AHR of subject #3, PHL of subject #4, AHL of subject #6, and AHR of subject #9.

[8] These definitions produced equal counts for both categories: SWR^+ (n = 1,170) and SWR^- (n = 1,170).

[9] These definitions result in equal durations for both categories: SWR^+ (93.0 [65.4] ms) and SWR^- (93.0 [65.4] ms).

[10] SWR^+ increased against the bootstrap sample; 95th percentile = 0.42 [Hz]; $p < 0.05$.

[11] SWR^+ (3.05 [0.85] SD of baseline, median [IQR]; n = 1,170) vs. SWR^- (2.37 [0.33] SD of baseline, median [IQR]; n = 1,170; $p < 0.001$; Brunner–Munzel test).

~~The magnitude of~~

As a result, $\|\text{mid-eSWR}^+\|$[12] exceeded ~~that of~~ $\|\text{pre-eSWR}^+\|$[13], and $\|\text{mid-rSWR}^+\|$[14] was larger than $\|\text{pre-rSWR}^+\|$ in both the Match IN and Mismatch OUT tasks.[15].

3.6. Visualization of hippocampal neural trajectory during SWR in two-dimensional spaces

Having observed neural trajectory 'jumping' during SWR (Figure 5), we visualized the three-dimensional trajectories of pre-, mid-, and post-SWR events during the encoding and retrieval phases (Figure 6). The distance between these was found to be memory-load dependent (Figure 3).

To provide two-dimensional visualization, we linearly aligned peri-SWR trajectories by setting g_E at the origin $(0, 0)$ and g_R at $(\|g_E g_R\|, 0)$. Subsequently, we rotated these aligned trajectories around the $g_E g_R$ axis (the x axis), ensuring that the distances from the origin in the original three-dimensional spaces and angles from $\overrightarrow{g_E g_R}$ are retained in the two-dimensional equivalent.

~~The scatter plot~~

Scatter plot visualization of neural trajectories within these two-dimensional spaces revealed ~~defining~~ distinct distributions of peri-SWR trajectories based on phases and task types. A ~~particular~~ notable example of this is ~~visible inCHEKME>one can observe<CHEKME~~ the observation that the magnitude of $\|\text{mid-eSWR}^+\|$ ~~surpasses~~ exceeds that of $\|\text{pre-eSWR}^+\|$ (Figure 6B), which is consistent with our previous observations (Figure 5).

3.7. Fluctuations of hippocampal neural trajectories between encoding and retrieval states

Subsequently, we ~~examined trajectory~~ investigated the 'direction' of the trajectory in relation to $\overrightarrow{g_E g_R}$, which was found to be dependent on memory load (Figure 3). The directions of ~~SWRs were defined~~ the SWRs were determined by the neural trajectory at -250

---

[12] 1.25 [1.30], median [IQR], $n = 1{,}281$ in ~~the~~ Match IN task; 1.12 [1.35], median [IQR], $n = 1{,}163$ in ~~the~~ Mismatch OUT task

[13] 1.08 [1.07], median [IQR], $n = 1{,}149$ in ~~the~~ Match IN task; 0.90 [1.12], median [IQR], $n = 1{,}088$ in ~~the~~ Mismatch OUT task

[14] 1.32 [1.24], median [IQR], $n = 935$ in ~~the~~ Match IN task; 1.15 [1.26], median [IQR], $n = 891$ in ~~the~~ Mismatch OUT task

[15] 1.19 [0.96], median [IQR], $n = 673$ in ~~the~~ Match IN task; 0.94 [0.88], median [IQR], $n = 664$ in ~~the~~ Mismatch OUT task

ms and $+250$ ms from their center, ~~i.e.~~ denoted as, for example, $\overrightarrow{\text{eSWR}^+}$. We calculated the cosine similarities between $\overrightarrow{g_E g_R}$, $\overrightarrow{\text{eSWR}}$, and $\overrightarrow{\text{rSWR}}$ in both SWR (SWR^+) and baseline periods (SWR^-) (Figure 7A – D).

$\overrightarrow{\text{rSWR}^+} \cdot \overrightarrow{g_E g_R}$ exhibited a biphasic distribution. By computing the difference between the distribution of $\overrightarrow{\text{rSWR}^+} \cdot \overrightarrow{g_E g_R}$ (Figure 7A & B) and that of $\overrightarrow{\text{rSWR}^-} \cdot \overrightarrow{g_E g_R}$ (Figure 7C & D), we were able to determine the contributions of SWR (Figure 7E & F), which indicated a shift in the direction of $\overrightarrow{g_E g_R}$ (Figure 7E & F: *red rectangles*).

Furthermore, $\overrightarrow{\text{eSWR}^+} \cdot \overrightarrow{\text{rSWR}^+}$ was less than $\overrightarrow{\text{eSWR}^-} \cdot \overrightarrow{\text{rSWR}^-}$ strictly in ~~the~~ Mismatch OUT task (Figure 7F: *pink circles*). In other words, eSWR and rSWR pointed in the opposite direction exclusively in ~~the~~ Mismatch OUT task but not ~~the~~ Match IN task (Figure 7E: *pink circles*).

4. Discussion

5. Discussion

This study hypothesizes that in low-dimensional spaces during a ~~working memory (WM)~~ WM task in humans, hippocampal neurons form unique trajectories, primarily during ~~sharp wave-ripple (SWR)~~ SWR periods. Initially, multiunit spikes in the ~~medial temporal lobe (MTL)~~ MTL regions were projected onto three-dimensional spaces during a Sternberg task using Gaussian-process factor analysis (GPFA) (Figure 1~~D — E and~~ D–E & Figure 2A). The trajectory ~~distance~~ distances across WM phases ($\|g_F g_E\|$, $\|g_F g_M\|$, $\|g_F g_R\|$, $\|g_E g_M\|$, $\|g_E g_R\|$, and $\|g_M g_R\|$) ~~was~~ were significantly larger in the hippocampus compared to the ~~entorhinal cortex (EC)~~ EC and amygdala (Figure 2E), indicating dynamic and responsive neural activity in the hippocampus during the WM task. Also, in the hippocampus, the trajectory distance between the encoding and retrieval phases ($\|g_F g_E\|$) correlated positively with memory load (Figure 3~~C — D~~ C–D), reflecting WM processing. The hippocampal neural trajectory transiently expanded during SWRs (Figure 5). Lastly, the hippocampal neural trajectory alternated between encoding and retrieval states, transitioning from encoding to retrieval during SWR events (Figure 7). These findings explain aspects of hippocampal neural activity during a WM task in humans and offer ~~FIXME>~~ new insights

into SWRs as a state-switching element in hippocampal neural states.

The distance of the neural trajectory across the phases was significantly longer in the hippocampus compared to the EC and amygdala, even when considering the distance from O in these regions (Figure 2C–E). This establishes the involvement of the hippocampus in the WM task, corroborating previous studies indicating hippocampal persistent firing during the maintenance phase [3] [4] [5] [6]. However, in the present study, applying GPFA to multiunit activity during a one-second level resolution of the WM task revealed that the neural trajectory in low-dimensional space presented a memory-load dependency between the encoding and retrieval phases, denoted as $\|g_E g_R\|$ (Figure 3). These findings support the association of the hippocampus with WM processing.

Our analysis focused on putative CA1 regions (Figure 4), is supported by several factors. This specific focus results from established observations that SWRs synchronize with interneuron and pyramidal neuron spike bursts [44] [45] [46] [47], potentially within a 50 μm radius of the recording site [48]. Furthermore, we identified an increased incidence of SWRs during the first 0–400 ms of the retrieval phase (Figure 4D). This finding aligns with previous reports of heightened SWR occurrence preceding spontaneous verbal recall [21] [22], supporting our results under a triggered retrieval condition. The observed log-normal distributions of both SWR duration and ripple band peak amplitude in this study (Figure 4C & E) coincide with the current consensus in this field [39]. Consequently, our decision to limit recording sites to putative CA1 regions likely contributed to improving the precision, or true positive rate, of SWR detection. Although, the trajectory distance increase from O during SWRs (Figure 5) might be artificially inflated towards higher values due to channel selection, this potential bias does not substantially challenge our main findings.

Interestingly, during the retrieval phase, trajectory directions alternated between encoding and retrieval states during both baseline and SWR periods in a task-dependent manner (Figure 7C & D). Additionally, the balance of this fluctuation transitioned from encoding to retrieval state during SWR events (Figure 7 E & F). These results align with previous studies on the role of SWR in memory retrieval [21] [22]. Our findings suggest that (i) neuronal oscillation between encoding and retrieval states occurs during a WM task and (ii) SWR events serve as indicators of the transition in hippocampal neural states from encoding to retrieval during a WM task.

Moreover, our study noted differences specific to the WM-task type between encoding- and retrieval-SWRs (Figure 7E–F). Notably, opposing movements of encoding-SWR (eSWR) and retrieval-SWR (rSWR) were not observed in Match IN task but were apparent in Mismatch OUT task. Memory engram theory [49] might explain these observations: Match In task presented participants with previously shown letters, while Mismatch OUT task introduced a new letter absent in the encoding phase. This explanation underscores the significant role of SWR in human cognitive processes.

In conclusion, this study illustrates that during a WM task in humans, hippocampal activity fluctuate between encoding and retrieval states, uniquely transitioning from encoding to retrieval during SWR events. These findings offer novel insights into the neural correlates and functionality of working memory within the hippocampus.

References

[1] W. B. Scoville, B. Milner, LOSS OF RECENT MEMORY AFTER BILATERAL HIPPOCAMPAL LESIONS, Journal of Neurology, Neurosurgery, and Psychiatry 20 (1) (1957) 11–21. URL https://www.ncbi.nlm.nih.gov/pmc/articles/PMC497229/

[2] L. R. Squire, The Legacy of Patient H.M. for Neuroscience, Neuron 61 (1) (2009) 6–9. doi:10.1016/j.neuron.2008.12.023. URL https://www.ncbi.nlm.nih.gov/pmc/articles/PMC2649674/

[3] E. Boran, T. Fedele, P. Klaver, P. Hilfiker, L. Stieglitz, T. Grunwald, J. Sarnthein, Persistent hippocampal neural firing and hippocampal-cortical coupling predict verbal working memory load, Science Advances 5 (3) (2019) eaav3687. doi:10.1126/sciadv.aav3687.

URL https://www.science.org/doi/10.1126/sciadv.aav3687

[4] J. Kamiński, S. Sullivan, J. M. Chung, I. B. Ross, A. N. Mamelak, U. Rutishauser, Persistently active neurons in human medial frontal and medial temporal lobe support working memory, Nature Neuroscience 20 (4) (2017) 590–601, number: 4 Publisher: Nature Publishing Group. doi:10.1038/nn.4509.
URL https://www.nature.com/articles/nn.4509

[5] S. Kornblith, R. Q. Quiroga, C. Koch, I. Fried, F. Mormann, Persistent Single-Neuron Activity during Working Memory in the Human Medial Temporal Lobe, Current Biology 27 (7) (2017) 1026–1032, publisher: Elsevier. doi:10.1016/j.cub.2017.02.013.
URL https://www.cell.com/current-biology/abstract/S0960-9822(17)30149-5

[6] M. C. M. Faraut, A. A. Carlson, S. Sullivan, O. Tudusciuc, I. Ross, C. M. Reed, J. M. Chung, A. N. Mamelak, U. Rutishauser, Dataset of human medial temporal lobe single neuron activity during declarative memory encoding and recognition, Scientific Data 5 (1) (2018) 180010, number: 1 Publisher: Nature Publishing Group. doi:10.1038/sdata.2018.10.
URL https://www.nature.com/articles/sdata201810

[7] A. A. Borders, C. Ranganath, A. P. Yonelinas, The hippocampus supports high-precision binding in visual working memory, Hippocampus 32 (3) (2022) 217–230. doi:10.1002/hipo.23401.

[8] J. Li, D. Cao, S. Yu, X. Xiao, L. Imbach, L. Stieglitz, J. Sarnthein, T. Jiang, Functional specialization and interaction in the amygdala-hippocampus circuit during working memory processing, Nature Communications 14 (1) (2023) 2921, number: 1 Publisher: Nature Publishing Group. doi:10.1038/s41467-023-38571-w.
URL https://www.nature.com/articles/s41467-023-38571-w

[9] V. Dimakopoulos, P. Mégevand, L. H. Stieglitz, L. Imbach, J. Sarnthein, Information flows from hippocampus to auditory cortex during replay of verbal working memory items, eLife 11 (2022) e78677, publisher: eLife Sciences Publications, Ltd. doi:10.7554/eLife.78677.
URL https://doi.org/10.7554/eLife.78677

[10] G. Buzsáki, Hippocampal sharp wave-ripple: A cognitive biomarker for episodic memory and planning, Hippocampus 25 (10) (2015) 1073–1188, _eprint: https://onlinelibrary.wiley.com/doi/pdf/10.1002/hipo.22488. doi:https://doi.org/10.1002/hipo.22488.
URL https://onlinelibrary.wiley.com/doi/abs/10.1002/hipo.22488

[11] M. A. Wilson, B. L. McNaughton, Reactivation of hippocampal ensemble memories during sleep, Science (New York, N.Y.) 265 (5172) (1994) 676–679. doi:10.1126/science.8036517.

[12] Z. Nádasdy, H. Hirase, A. Czurkó, J. Csicsvari, G. Buzsáki, Replay and Time Compression of Recurring Spike Sequences in the Hippocampus, Journal of Neuroscience 19 (21) (1999) 9497–9507, publisher: Society for Neuroscience Section: ARTICLE. doi:10.1523/JNEUROSCI.19-21-09497.1999.
URL https://www.jneurosci.org/content/19/21/9497

[13] A. K. Lee, M. A. Wilson, Memory of sequential experience in the hippocampus during slow wave sleep, Neuron 36 (6) (2002) 1183–1194. doi:10.1016/s0896-6273(02)01096-6.

[14] K. Diba, G. Buzsáki, Forward and reverse hippocampal place-cell sequences during ripples, Nature Neuroscience 10 (10) (2007) 1241–1242, number: 10 Publisher: Nature Publishing Group. doi:10.1038/nn1961.
URL https://www.nature.com/articles/nn1961

[15] T. J. Davidson, F. Kloosterman, M. A. Wilson, Hippocampal replay of extended experience, Neuron 63 (4) (2009) 497–507. doi:10.1016/j.neuron.2009.07.027.

[16] G. Girardeau, K. Benchenane, S. I. Wiener, G. Buzsáki, M. B. Zugaro, Selective suppression of hippocampal ripples impairs spatial memory, Nature Neuroscience 12 (10) (2009) 1222–1223. doi:10.1038/nn.2384.
URL http://www.nature.com/articles/nn.2384

[17] V. Ego-Stengel, M. A. Wilson, Disruption of ripple-associated hippocampal activity during rest impairs spatial learning in the rat, Hippocampus 20 (1) (2010) 1–10. doi:10.1002/hipo.20707.

[18] A. Fernández-Ruiz, A. Oliva, E. Fermino de Oliveira, F. Rocha-Almeida, D. Tingley, G. Buzsáki, Long-duration hippocampal sharp wave ripples improve memory, Science (New York, N.Y.) 364 (6445) (2019) 1082–1086. doi:10.1126/science.aax0758.
URL https://www.ncbi.nlm.nih.gov/pmc/articles/PMC6693581/

[19] J. Kim, A. Joshi, L. Frank, K. Ganguly, Cortical–hippocampal coupling during manifold exploration in motor cortex, Nature (2022) 1–8Publisher: Nature Publishing Group. doi:10.1038/s41586-022-05533-z.
URL https://www.nature.com/articles/s41586-022-05533-z

[20] C.-T. Wu, D. Haggerty, C. Kemere, D. Ji, Hippocampal awake replay in fear memory retrieval, Nature Neuroscience 20 (4) (2017) 571–580. doi:10.1038/nn.4507.

[21] Y. Norman, E. M. Yeagle, S. Khuvis, M. Harel, A. D. Mehta, R. Malach, Hippocampal sharp-wave ripples linked to visual episodic recollection in humans, Science 365 (6454) (2019) eaax1030. doi:10.1126/science.aax1030.
URL https://www.sciencemag.org/lookup/doi/10.1126/science.aax1030

[22] Y. Norman, O. Raccah, S. Liu, J. Parvizi, R. Malach, Hippocampal ripples and their coordinated dialogue with the default mode network during recent and remote recollection, Neuron 109 (17) (2021) 2767–2780.e5, publisher: Elsevier. doi:10.1016/j.neuron.2021.06.020.
URL https://www.cell.com/neuron/abstract/S0896-6273(21)00461-X

[23] C. J. Behrens, L. P. van den Boom, L. de Hoz, A. Friedman, U. Heinemann, Induction of sharp wave–ripple complexes in vitro and reorganization of hippocampal networks, Nature Neuroscience 8 (11) (2005) 1560–1567, number: 11 Publisher: Nature Publishing Group. doi:10.1038/nn1571.
URL https://www.nature.com/articles/nn1571

[24] H. Norimoto, K. Makino, M. Gao, Y. Shikano, K. Okamoto, T. Ishikawa, T. Sasaki, H. Hioki, S. Fujisawa, Y. Ikegaya, Hippocampal ripples down-regulate synapses, Science (New York, N.Y.) 359 (6383) (2018) 1524–1527. doi:10.1126/science.

aao0702.

[25] S. P. Jadhav, C. Kemere, P. W. German, L. M. Frank, Awake Hippocampal Sharp-Wave Ripples Support Spatial Memory, Science 336 (6087) (2012) 1454–1458, publisher: American Association for the Advancement of Science. doi:10.1126/science.1217230.
URL https://www.science.org/doi/abs/10.1126/science.1217230

[26] J. O'Keefe, J. Dostrovsky, The hippocampus as a spatial map: Preliminary evidence from unit activity in the freely-moving rat, Brain Research 34 (1971) 171–175, place: Netherlands Publisher: Elsevier Science. doi:10.1016/0006-8993(71)90358-1.

[27] J. O'Keefe, Place units in the hippocampus of the freely moving rat, Experimental Neurology 51 (1) (1976) 78–109. doi:10.1016/0014-4886(76)90055-8.
URL https://www.sciencedirect.com/science/article/pii/0014488676900558

[28] A. D. Ekstrom, M. J. Kahana, J. B. Caplan, T. A. Fields, E. A. Isham, E. L. Newman, I. Fried, Cellular networks underlying human spatial navigation, Nature 425 (6954) (2003) 184–188, number: 6954 Publisher: Nature Publishing Group. doi:10.1038/nature01964.
URL https://www.nature.com/articles/nature01964

[29] K. B. Kjelstrup, T. Solstad, V. H. Brun, T. Hafting, S. Leutgeb, M. P. Witter, E. I. Moser, M.-B. Moser, Finite Scale of Spatial Representation in the Hippocampus, Science 321 (5885) (2008) 140–143, publisher: American Association for the Advancement of Science. doi:10.1126/science.1157086.
URL https://www.science.org/doi/abs/10.1126/science.1157086

[30] C. D. Harvey, F. Collman, D. A. Dombeck, D. W. Tank, Intracellular dynamics of hippocampal place cells during virtual navigation, Nature 461 (7266) (2009) 941–946, number: 7266 Publisher: Nature Publishing Group. doi:10.1038/nature08499.
URL https://www.nature.com/articles/nature08499

[31] H. Zhang, P. D. Rich, A. K. Lee, T. O. Sharpee, Hippocampal spatial representations exhibit a hyperbolic geometry that expands with experience, Nature Neuroscience (Dec. 2022). doi:10.1038/s41593-022-01212-4.
URL https://www.nature.com/articles/s41593-022-01212-4

[32] P. A. Naber, F. H. Lopes da Silva, M. P. Witter, Reciprocal connections between the entorhinal cortex and hippocampal fields CA1 and the subiculum are in register with the projections from CA1 to the subiculum, Hippocampus 11 (2) (2001) 99–104, _eprint: https://onlinelibrary.wiley.com/doi/pdf/10.1002/hipo.1028. doi:10.1002/hipo.1028.
URL https://onlinelibrary.wiley.com/doi/abs/10.1002/hipo.1028

[33] N. M. van Strien, N. L. M. Cappaert, M. P. Witter, The anatomy of memory: an interactive overview of the parahippocampal–hippocampal network, Nature Reviews Neuroscience 10 (4) (2009) 272–282, number: 4 Publisher: Nature Publishing Group. doi:10.1038/nrn2614.
URL https://www.nature.com/articles/nrn2614

[34] B. A. Strange, M. P. Witter, E. S. Lein, E. I. Moser, Functional organization of the hippocampal longitudinal axis, Nature Reviews Neuroscience 15 (10) (2014) 655–669, number: 10 Publisher: Nature Publishing Group. doi:10.1038/nrn3785.
URL https://www.nature.com/articles/nrn3785

[35] R. J. Gardner, E. Hermansen, M. Pachitariu, Y. Burak, N. A. Baas, B. A. Dunn, M.-B. Moser, E. I. Moser, Toroidal topology of population activity in grid cells, Nature 602 (7895) (2022) 123–128, number: 7895 Publisher: Nature Publishing Group. doi:10.1038/s41586-021-04268-7.
URL https://www.nature.com/articles/s41586-021-04268-7

[36] E. Boran, T. Fedele, A. Steiner, P. Hilfiker, L. Stieglitz, T. Grunwald, J. Sarnthein, Dataset of human medial temporal lobe neurons, scalp and intracranial EEG during a verbal working memory task, Scientific Data 7 (1) (2020) 30, number: 1 Publisher: Nature Publishing Group. doi:10.1038/s41597-020-0364-3.
URL https://www.nature.com/articles/s41597-020-0364-3

[37] B. M. Yu, J. P. Cunningham, G. Santhanam, S. I. Ryu, K. V. Shenoy, M. Sahani, Gaussian-Process Factor Analysis for Low-Dimensional Single-Trial Analysis of Neural Population Activity, Journal of Neurophysiology 102 (1) (2009) 614–635. doi:10.1152/jn.90941.2008.
URL https://www.ncbi.nlm.nih.gov/pmc/articles/PMC2712272/

[38] J. Niediek, J. Boström, C. E. Elger, F. Mormann, Reliable Analysis of Single-Unit Recordings from the Human Brain under Noisy Conditions: Tracking Neurons over Hours, PLOS ONE 11 (12) (2016) e0166598, publisher: Public Library of Science. doi:10.1371/journal.pone.0166598.
URL https://journals.plos.org/plosone/article?id=10.1371/journal.pone.0166598

[39] A. A. Liu, S. Henin, S. Abbaspoor, A. Bragin, E. A. Buffalo, J. S. Farrell, D. J. Foster, L. M. Frank, T. Gedankien, J. Gotman, J. A. Guidera, K. L. Hoffman, J. Jacobs, M. J. Kahana, L. Li, Z. Liao, J. J. Lin, A. Losonczy, R. Malach, M. A. van der Meer, K. McClain, B. L. McNaughton, Y. Norman, A. Navas-Olive, L. M. de la Prida, J. W. Rueckemann, J. J. Sakon, I. Skelin, I. Soltesz, B. P. Staresina, S. A. Weiss, M. A. Wilson, K. A. Zaghloul, M. Zugaro, G. Buzsáki, A consensus statement on detection of hippocampal sharp wave ripples and differentiation from other fast oscillations, Nature Communications 13 (1) (2022) 6000, number: 1 Publisher: Nature Publishing Group. doi:10.1038/s41467-022-33536-x.
URL https://www.nature.com/articles/s41467-022-33536-x

[40] K. Kay, M. Sosa, J. E. Chung, M. P. Karlsson, M. C. Larkin, L. M. Frank, A hippocampal network for spatial coding during immobility and sleep, Nature 531 (7593) (2016) 185–190. doi:10.1038/nature17144.

[41] L. McInnes, J. Healy, N. Saul, L. Großberger, UMAP: Uniform Manifold Approximation and Projection, Journal of Open Source Software 3 (29) (2018) 861. doi:10.21105/joss.00861.
URL https://joss.theoj.org/papers/10.21105/joss.00861

[42] P. J. Rousseeuw, Silhouettes: A graphical aid to the interpretation and validation of cluster analysis, Journal of

Computational and Applied Mathematics 20 (1987) 53–65. `doi:10.1016/0377-0427(87)90125-7`.
URL `https://www.sciencedirect.com/science/article/pii/0377042787901257`

[43] P. Virtanen, R. Gommers, T. E. Oliphant, M. Haberland, T. Reddy, D. Cournapeau, E. Burovski, P. Peterson, W. Weckesser, J. Bright, S. J. van der Walt, M. Brett, J. Wilson, K. J. Millman, N. Mayorov, A. R. J. Nelson, E. Jones, R. Kern, E. Larson, C. J. Carey, Polat, Y. Feng, E. W. Moore, J. VanderPlas, D. Laxalde, J. Perktold, R. Cimrman, I. Henriksen, E. A. Quintero, C. R. Harris, A. M. Archibald, A. H. Ribeiro, F. Pedregosa, P. van Mulbregt, SciPy 1. 0 Contributors, SciPy 1.0: fundamental algorithms for scientific computing in Python, Nature Methods 17 (2020) 261–272, aDS Bibcode: 2020NatMe..17..261V. `doi:10.1038/s41592-019-0686-2`.
URL `https://ui.adsabs.harvard.edu/abs/2020NatMe..17..261V`

[44] G. Buzsáki, Two-stage model of memory trace formation: a role for "noisy" brain states, Neuroscience 31 (3) (1989) 551–570. `doi:10.1016/0306-4522(89)90423-5`.

[45] M. L. V. Quyen, A. Bragin, R. Staba, B. Crépon, C. L. Wilson, J. Engel, Cell Type-Specific Firing during Ripple Oscillations in the Hippocampal Formation of Humans, Journal of Neuroscience 28 (24) (2008) 6104–6110, publisher: Society for Neuroscience Section: Brief Communications. `doi:10.1523/JNEUROSCI.0437-08.2008`.
URL `https://www.jneurosci.org/content/28/24/6104`

[46] S. Royer, B. V. Zemelman, A. Losonczy, J. Kim, F. Chance, J. C. Magee, G. Buzsáki, Control of timing, rate and bursts of hippocampal place cells by dendritic and somatic inhibition, Nature Neuroscience 15 (5) (2012) 769–775, number: 5 Publisher: Nature Publishing Group. `doi:10.1038/nn.3077`.
URL `https://www.nature.com/articles/nn.3077`

[47] N. Hájos, M. R. Karlócai, B. Németh, I. Ulbert, H. Monyer, G. Szabó, F. Erdélyi, T. F. Freund, A. I. Gulyás, Input-output features of anatomically identified CA3 neurons during hippocampal sharp wave/ripple oscillation in vitro, The Journal of Neuroscience: The Official Journal of the Society for Neuroscience 33 (28) (2013) 11677–11691. `doi:10.1523/JNEUROSCI.5729-12.2013`.

[48] E. W. Schomburg, C. A. Anastassiou, G. Buzsáki, C. Koch, The Spiking Component of Oscillatory Extracellular Potentials in the Rat Hippocampus, The Journal of Neuroscience 32 (34) (2012) 11798–11811. `doi:10.1523/JNEUROSCI.0656-12.2012`.
URL `https://www.ncbi.nlm.nih.gov/pmc/articles/PMC3459239/`

[49] X. Liu, S. Ramirez, P. T. Pang, C. B. Puryear, A. Govindarajan, K. Deisseroth, S. Tonegawa, Optogenetic stimulation of a hippocampal engram activates fear memory recall, Nature 484 (7394) (2012) 381–385, number: 7394 Publisher: Nature Publishing Group. `doi:10.1038/nature11028`.
URL `https://www.nature.com/articles/nature11028`

Contributors

Y.W. and T.Y. conceptualized the study; Y.W. performed the data analysis; Y.W. and T.Y. wrote the original draft; and all authors reviewed the final manuscript.

Acknowledgments

Declaration of Interests

The authors declare that they have no competing interests.

Data and code availability

The data is available on G-Node (`https://doi.gin.g-node.org/10.12751/g-node.d76994/`).
The source code is available on GitHub (`https://github.com/yanagisawa-lab/hippocampal-neural-fluctuation-during-a-WM-task-in-hum`

Inclusion and Diversity Statement

We support inclusive, diverse, and equitable conduct of research.

Declaration of Generative AI in Scientific Writing

The authors employed ChatGPT, provided by OpenAI, for enhancing the manuscript's English language quality. After incorporating the suggested improvements, the authors meticulously revised the content. Ultimate responsibility for the final content of this publication rests entirely with the authors.

Tables

Subject ID	of sessions	AHL	AHR	PHL	PHR	ECL	ECR	AL	AR	SOZ
1	4									"AHR, LR"
2	7									"AHR, PHR"
3	3									"AHL, PHL"
4	2									"AHL, AHR, PHL, PHR"
5	3									DRR
6	6									"AHL, PHL, ECL, AL"
7	4									"AHR, PHR"
8	5									ECR
9	2									"ECR, AR"

Table 1 – Electrode Distribution within the Dataset

This figure denotes the placements of electrodes and seizure onset zones. Regions marked with were included in the dataset, while those imprinted with were absent. The abbreviations used are as follows: AHL, left hippocampal head; AHR, right hippocampal head; PHL, left hippocampal body; PHR, right hippocampal body; ECL, left entorhinal cortex; ECR, right entorhinal cortex; AL, left amygdala; AR, right amygdala; SOZ represents the seizure onset zone.

Subject	AHL	AHR	PHL	PHR
1	0.60 ± 0.14	n.a.	n.a.	0.1 ± 0
2	0.21 ± 0.16	0.17 ± 0.21	0.18 ± 0.22	0.20 ± 0.15
3	0.40 ± 0.42	0.83 ± 0.12	n.a.	n.a.
4	0.10 ± 0.00	0.10 ± 0.00	0.90 ± 0.00	0.10 ± 0.14
5	n.a.	n.a.	n.a.	n.a.
6	0.63 ± 0.06	n.a.	n.a.	0.27 ± 0.06
7	0.10 ± 0.00	0.35 ± 0.35	0.37 ± 0.47	0.10 ± 0.00
8	0.13 ± 0.10	n.a.	0.28 ± 0.49	n.a.
9	n.a.	0.85 ± 0.07	0.15 ± 0.07	n.a.

Table 2 – Silhouette score of UMAP clustering for SWR^+ candidates and SWR^- candidates

The silhouette scores (mean ±SD across sessions per subject) for UMAP clustering of SWR^+ candidates and SWR^- candidates are based on their respective multiunit spike patterns (Figure 4A). The mean scores were 0.205 and the standard deviation was 0.285, calculated for the interquartile range (IQR; Figure 4B).

Subject ID	of sessions	of trials	ROI	of SWRs	SWR incidence [Hz]
#1	2	100	AHL	274	0.34
#3	2	97	AHR	325	0.42
#4	2	99	PHL	202	0.26
#6	2	100	AHL	297	0.37
#9	2	97	AHR	72	0.09
Total = 10	Total = 493	Total = 1170	0.30 ± 0.13 (mean ± SD)		

Table 3 – Summary of Detected SWR Events

The table provides statistics of presumptive CA1 regions and SWR events. Only the initial two sessions (sessions 1 and 2) from each subject were included in our analysis to reduce sampling bias.
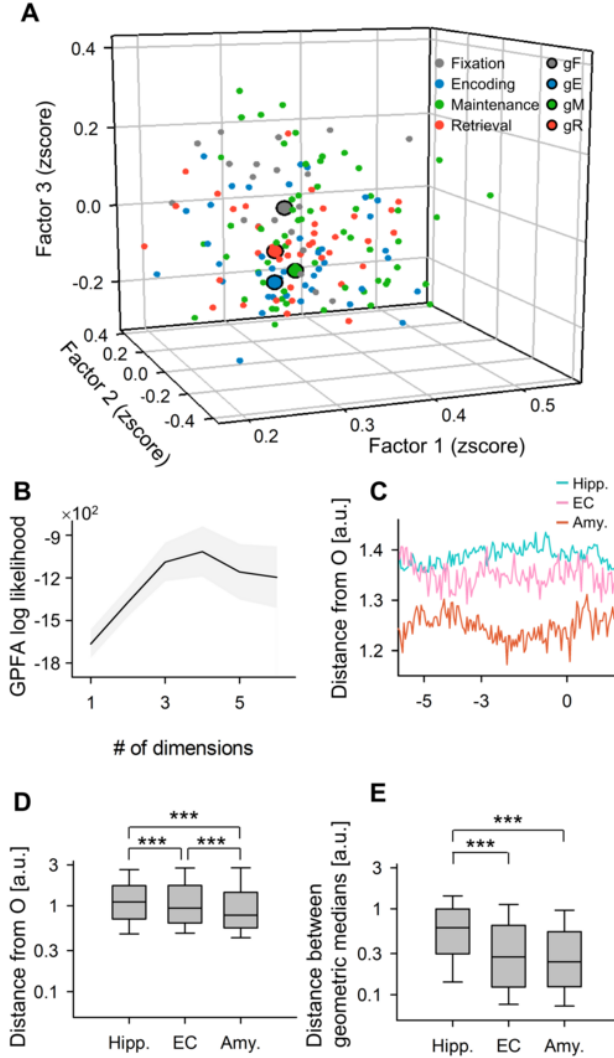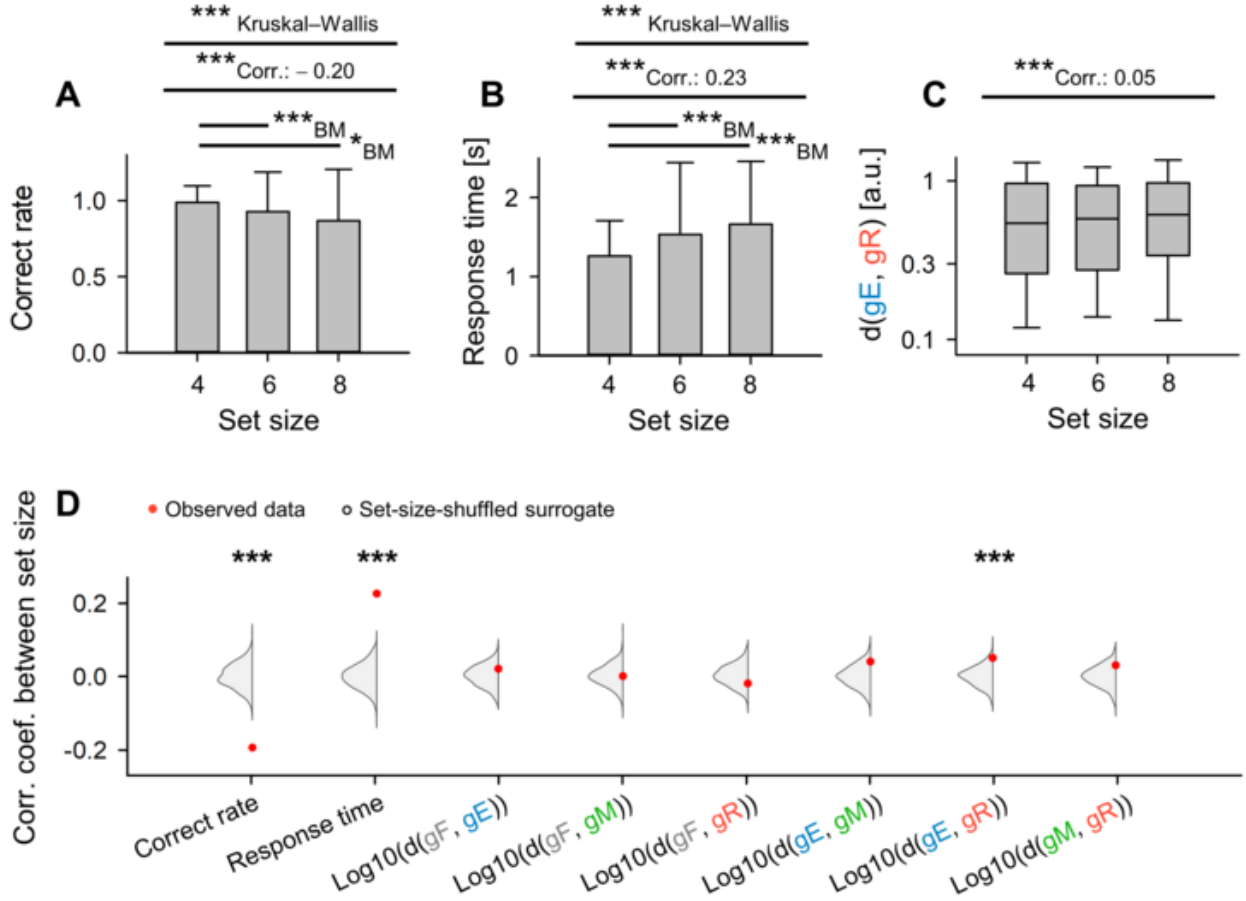
Figures
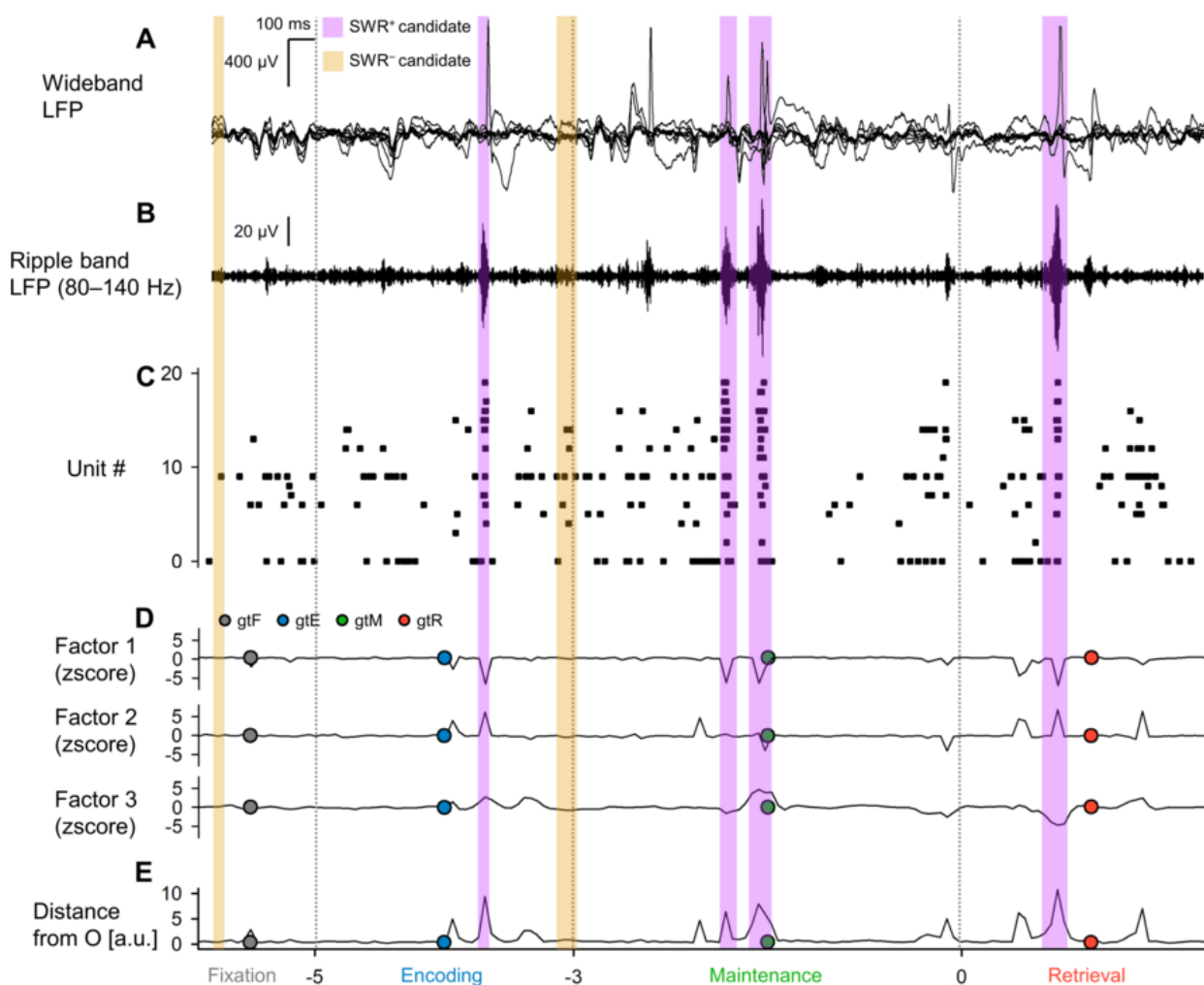
Figure 1 – Local Field Potentials (LFP), Multiunit Activity, and Neural Trajectories in the Hippocampus During a Modified Sternberg Task

A. Representative wideband LFP signals for intracranial EEG recording from the left hippocampal head are presented. This recording took place while the subject performed a modified Sternberg working memory task. Task stages included fixation (1 s, *gray*), encoding (2 s, *blue*), maintenance (3 s, *green*), and retrieval (2 s, *red*). ***B.*** Displays the associated ripple band LFP traces. Note *purple* and *yellow* rectangles, which denote the timings for SWR⁺ candidates and SWR⁻ candidates, respectively (the latter serving as control events for SWR⁺). ***C.*** A raster plot illustrates multiunit spikes from the LFP traces. These spikes have been sorted using a spike algorithm [38]. ***D.*** Shows neural trajectories computed by GPFA[37] based on spike counts per unit with 50-ms bins. The geometric median of each phase is marked by dot circles. ***E.*** Indicates the distance of the neural trajectory from the origin point *O*.

Figure 2 – State-Dependent Trajectories of Hippocampal Neurons

A. Neural trajectories ~~are depicted~~ as a point cloud within the ~~initial~~ first three-dimensional factors derived from Gaussian Process Factor Analysis (GPFA) [37]. The smaller dots ~~correspond to coordinates of~~ represent 50-ms neural trajectory bins, ~~while~~ and the larger dots with *black* edges ~~show~~ denote the geometric medians for ~~respective phases~~ each phase in the Sternberg working memory task: fixation ($\|g_F\|$, *gray*), encoding ($\|g_E\|$, *blue*), maintenance ($\|g_M\|$, *green*), and retrieval ($\|g_R\|$, *red*). **B.** The figure ~~conveys~~ presents the log-likelihood of the GPFA models versus the ~~count~~ number of dimensions used to embed multiunit spikes found in the medial temporal lobe (MTL) ~~territories~~ regions. ~~In specific~~ Specifically, the elbow method ~~pinpointed~~ identified three as the optimal dimension ~~to be three~~. **C.** This panel ~~illustrates~~ displays the distance of the neural trajectories from the origin (*O*) for the hippocampus (Hipp.), entorhinal cortex (EC), and amygdala (Amy.), plotted against the time elapsed from the probe onset. **D.** The ~~distance of the~~ trajectory distance from *O* within the MTL regions is ~~displayed~~ shown. The hippocampus ~~shows~~ has the ~~farthest~~ greatest distance, followed by the EC and the Amygdala. **E.** The box plot ~~represents~~ illustrates inter-phase trajectory distances within the MTL regions.

Figure 3 – ~~Dependency of Trajectory Distance on Memory Load: Encoding and Retrieval States in Hippocampus~~ **Relationship between Trajectory Distance and Memory Load: States of Encoding and Retrieval in the Hippocampus**

A. ~~The~~ Demonstrates the relationship between set size (number of letters ~~that need~~ to be encoded) and ~~correct rate~~ accuracy in the working memory task (coefficient = −0.20, ***$p < 0.001$). **B.** ~~The~~ Displays the correlation between set size and response time (coefficient = 0.23, ***$p < 0.001$). **C.** ~~The impact~~ Exhibits the influence of set size on the inter-phase distances between the encoding and retrieval phases ($\|g_E g_R\|$) (correlation coefficient = 0.05, ***$p < 0.001$). **D.** *Red* ~~dots represent~~ Indicates experimental observations of correlations between set size and the following parameters: ~~correct rate~~accuracy, response time, $\log_{10}\|g_F g_E\|$, $\log_{10}\|g_F g_M\|$, $\log_{10}\|g_F g_R\|$, $\log_{10}\|g_E g_M\|$, $\log_{10}\|g_E g_R\|$, and $\log_{10}\|g_M g_R\|$ represented by *red* dots. The *gray* kernel density plots illustrate the corresponding ~~set-size-shuffled~~ shuffled surrogate with set size ($n = 1{,}000$) (***ps < 0.001).

Figure 4 – **Detection of SWRs in Presumptive CA1 Regions**

A. Two-dimensional UMAP [41] projection displays multi-unit spikes during SWR$^+$ candidates (*purple*) and SWR$^-$ candidates (*yellow*). **B.** A cumulative density plot indicates silhouette scores, reflecting UMAP clustering quality (see Table 2). Hippocampal regions with silhouette scores exceeding 0.60 (equivalent to the 75th percentile) are identified as putative CA1 regions. SWR$^+$ and SWR$^-$ candidates, which were recorded from these regions, are classified as SWR$^+$ and SWR$^-$ respectively (*n*s = 1,170). **C.** Identical distributions of durations are presented for SWR$^+$ (*purple*) and SWR$^-$ (*yellow*), based on their definitions (93.0 [65.4] ms, median [IQR]). **D.** SWR incidence for both SWR$^+$ (*purple*) and SWR$^-$ (*yellow*), relative to the probe's timing, is illustrated as a mean ±95% confidence interval. However, intervals may not be visibly apparent due to their confined ranges, be aware that a significant SWR incidence increase was detected during the initial 400 ms of the retrieval phase (0.421 [Hz], *$p < 0.05$, bootstrap test). **E.** Distributions of ripple band peak amplitudes for SWR$^-$ (*yellow*; 2.37 [0.33] SD of baseline, median [IQR]) and SWR$^+$ (*purple*; 3.05 [0.85] SD of baseline, median [IQR]) are manifested (***$p < 0.001$, the Brunner–Munzel test).
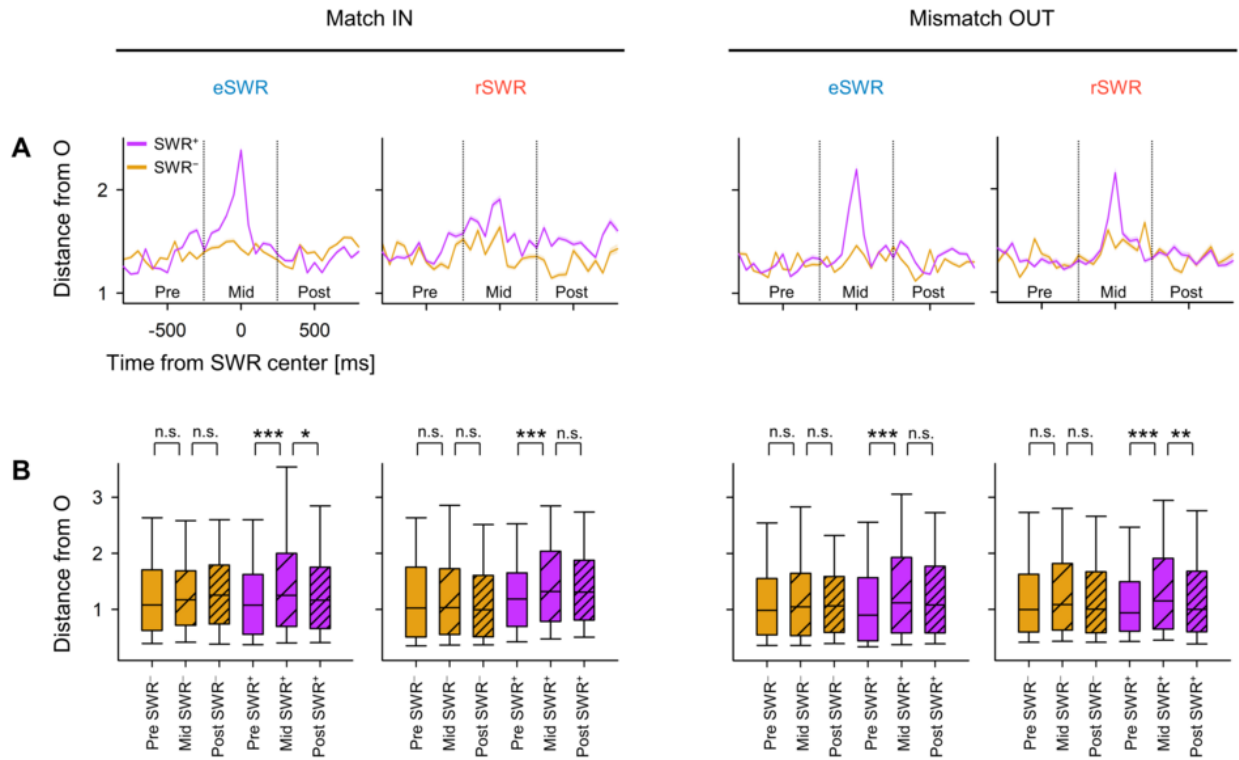
Figure 5 – ~~Transient Alterations in Neural Trajectory During SWR Events~~ <u>Transient Changes in Neural Pathway During SWR Events</u>

A. ~~Displayed~~ <u>Presented</u> is the distance from origin (O) of the peri-sharp-wave-ripple ~~trajectory~~ <u>pathway</u> (mean ±95% confidence interval). The intervals may ~~not~~ be ~~apparent~~ <u>obscured</u> due to their ~~narrow~~ <u>minimal</u> ranges. *B.* ~~Shown is the~~ <u>The</u> distance from the origin (O) during <u>the</u> pre-, mid-, and post-SWR periods <u>is demonstrated</u> (*$p < 0.05$, **$p < 0.01$, ***$p < 0.001$; ~~the~~ Brunner–Munzel test <u>applied</u>). Abbreviations: SWR, sharp-wave ripple events; eSWR, SWR during the encoding phase; rSWR, SWR ~~while in~~ <u>within</u> the retrieval phase; SWR$^+$, positive SWR event; SWR$^-$, control events for SWR$^+$; pre-, mid-, or post-SWR ~~denote~~ <u>refer to</u> the time intervals from -800 to -250 ms, from -250 to $+250$ ms, or from $+250$ to $+800$ ms, <u>respectively,</u> all relative to the ~~center of the~~ SWR <u>center</u>.
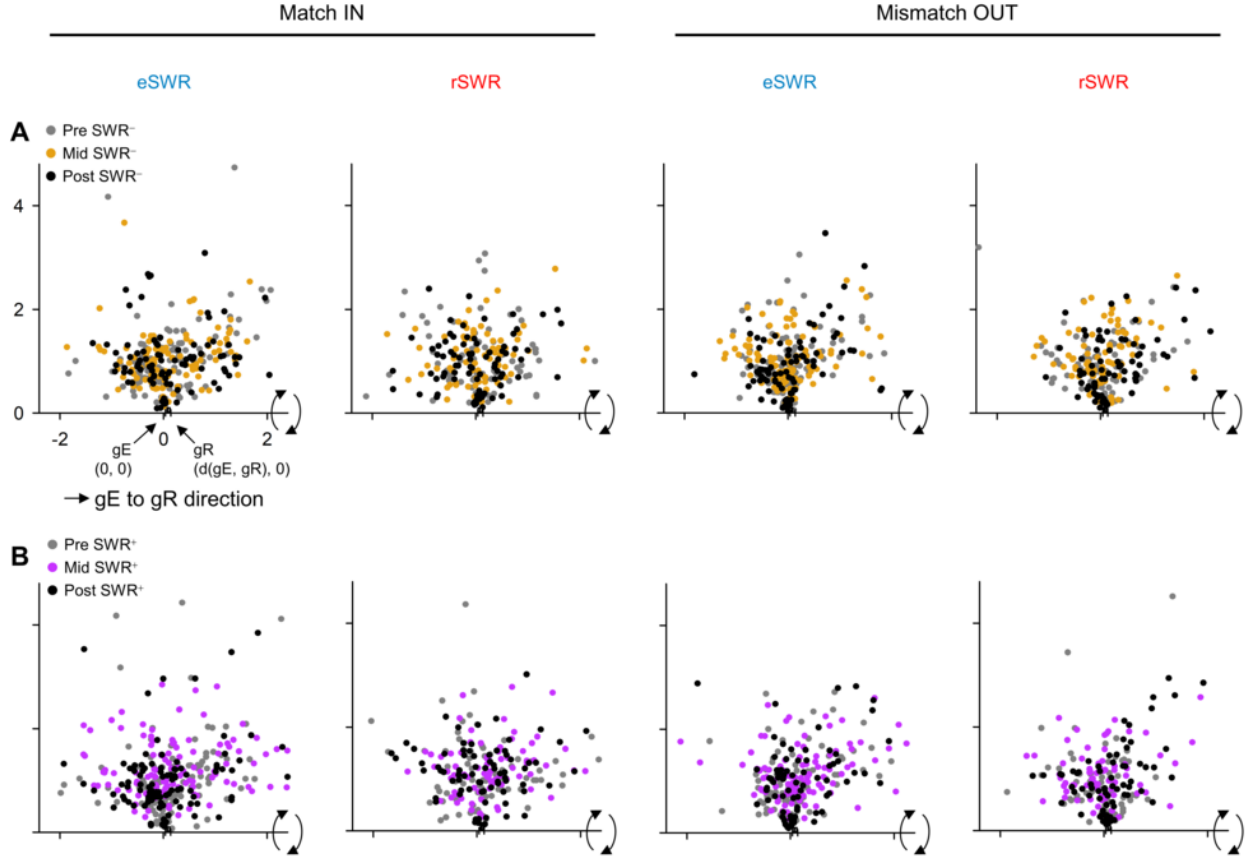
Figure 6 – Visualization of Neural Trajectories during SWR in Two-Dimensional Spaces

The panels ~~display~~ depict hippocampal neural trajectories during SWR ~~as~~ projected onto two-dimensional spaces. **A.** ~~Hippocampal~~ Shows the hippocampal neural trajectories as point clouds during pre-SWR$^-$ (*gray*), mid-SWR$^-$ (*yellow*), and post-SWR$^-$ (*black*). **B.** ~~Represents~~ Conveys the ~~equivalents~~ equivalent for SWR$^+$ ~~as opposed to~~ rather than SWR$^-$. The projection was ~~applied in the following manner~~ executed as follows: First, a linear transformation ~~positioned~~ placed g_E at the origin O (0,0), and g_R at ($\|g_E g_R\|$, 0). The point cloud was ~~then~~ subsequently rotated around the $g_E g_R$ axis (~~equivalent~~ similar to the x axis) for ~~fitting into~~ adaptation to two-dimensional spaces. ~~Therefore~~Thus, within these two-dimensional spaces, ~~both~~ the distances from point O and the angles for the $g_E g_R$ axis are ~~preserved~~ retained as in the original ~~three dimensional~~ three-dimensional spaces ~~in~~ created by GPFA. Abbreviations: SWR ~~signifies~~ denotes sharp-wave ripple events; eSWR ~~denotes~~ refers to SWR during the encoding phase; rSWR ~~indicates~~ signals SWR during the retrieval phase; SWR$^+$, ~~marks~~ characterizes an SWR event; SWR$^-$ ~~refers to~~ signifies control events for SWR$^+$; pre-SWR, mid-SWR, or post-SWR, ~~reference~~ represent the time intervals from −800 to −250 ms, from −250 to +250 ms, or from +250 to +800 ms from the center of the SWR.

20
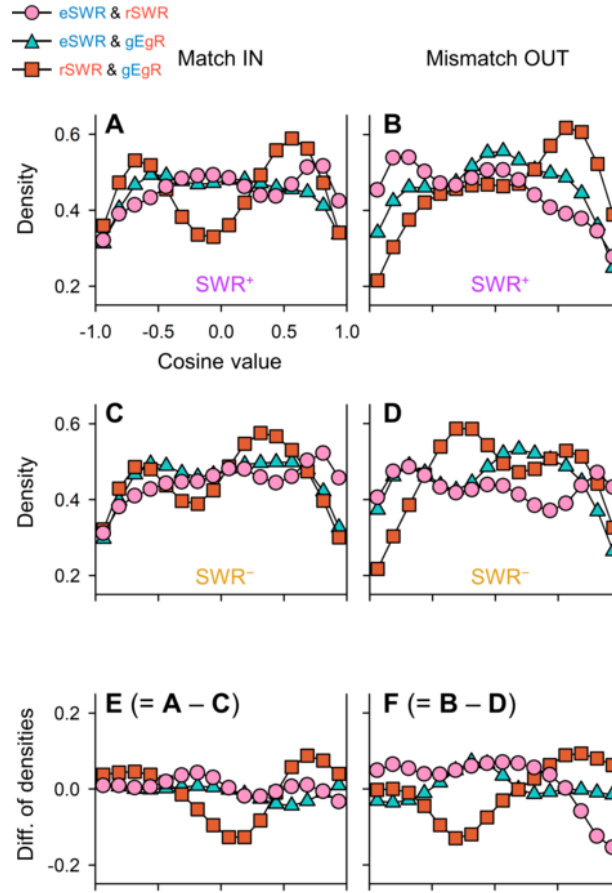
Figure 7 – ~~Directions of Neural Trajectories during SWRs Based on Encoding and Retrieval States~~ **Neural Trajectories Direction during SWRs Based on Encoding and Retrieval States**

A–B ~~Kernel~~ Shows the kernel density estimation distributions of $\overrightarrow{\text{eSWR}^\pm} \cdot \overrightarrow{\text{rSWR}^\pm}$ $\overrightarrow{\text{eSWR}^+} \cdot \overrightarrow{\text{rSWR}^+}$ (*pink circles* depicted as pink circles), $\overrightarrow{\text{eSWR}^\pm} \cdot \overrightarrow{\text{g}_E\text{g}_R}$ $\overrightarrow{\text{eSWR}^+} \cdot \overrightarrow{\text{g}_E\text{g}_R}$ (*blue triangles* blue triangles), and $\overrightarrow{\text{rSWR}^\pm} \cdot \overrightarrow{\text{g}_E\text{g}_R}$ $\overrightarrow{\text{rSWR}^+} \cdot \overrightarrow{\text{g}_E\text{g}_R}$ (*red rectangles* red rectangles) in ~~the~~ Match In (*A*) and Mismatch OUT tasks (*B*). ***C–D*** ~~Present~~ Illustrates the corresponding distributions of SWR⁻ instead of those of SWR⁺ in *A* and *B*. ***E–F*** ~~Depict~~ Renders the differences in the distributions of SWR⁺ and SWR⁻, ~~illuminating~~ detailing the SWR components (*E* = *C* ~~—~~ *A* ~~&~~ *F* = *D* ~~—~~ *B*). ~~Note the~~ The biphasic distributions of $\overrightarrow{\text{rSWR}^-} \cdot \overrightarrow{\text{g}_E\text{g}_R}$, ~~suggesting~~ $\overrightarrow{\text{rSWR}^-} \cdot \overrightarrow{\text{g}_E\text{g}_R}$ indicates fluctuations between the encoding and retrieval states during the Sternberg task. ~~Moreover~~Also, ~~inverse~~ contradicting directionality between $\overrightarrow{\text{eSWR}^+}$ and $\overrightarrow{\text{rSWR}^+}$ was observed (*pink circles* pink circles) not in the Match IN task (*E*)~~)~~, but in Mismatch OUT task (*F*). Lastly, ~~Finally, shifts~~ transition from the retrieval to encoding states are ~~acknowledged~~ apparent in the SWR components in both Match IN and Mismatch OUT tasks (*red rectangles* red rectangles in *E–F*).

21